Thin-Walled Structures 183 (2023) 110380

Contents lists available at ScienceDirect

Thin-Walled Structures

journal homepage: www.elsevier.com/locate/tws

Full length article

Advanced numerical modelling for predicting residual compressive strength of corroded stiffened plates

Krzysztof Woloszyk [a], Yordan Garbatov [b,*]

[a] Institute of Ocean Engineering and Ship Technology, Gdansk University of Technology, G. Narutowicza 11/12 st., 80-233, Gdansk, Poland
[b] Centre for Marine Technology and Ocean Engineering (CENTEC), Instituto Superior Técnico, Universidade de Lisboa, Avenida Rovisco Pais, 1049-001, Lisboa, Portugal

ARTICLE INFO

Keywords:
Corrosion
Random field
Stiffened plate
Ultimate strength
FEM

ABSTRACT

An advanced methodology for predicting the residual compressive strength of corroded stiffened plates is developed here using the non-linear finite element method. The non-uniform loss of a plate thickness is accounted for on a macro-scale. In contrast, mechanical properties are changed using the constitutive model to reflect the corrosion degradation impact on a micro-scale. Three different stiffened plate thicknesses are considered, and ultimate compressive capacity is analysed for different severity of corrosion degradation. First, the deterministic analysis is performed, and numerical results are validated against the experiment. Then, the corrosion fields are modelled with the use of random fields. Different statistical characteristics of the generated random fields are investigated to identify their impact on the resulting structural behaviour. It was found that severe corrosion degradation could cause an excessive reduction of structural capacity even at 50%. Finally, the results of the present study are compared with the already studied corrosion models showing a highly non-conservative solution of the latter, where the plate thickness is reduced only due to the corrosion degradation progress.

1. Introduction

Ships and offshore structures are subjected to a severe corrosion environment [1] since there are operating in seawater, which is considered a highly corrosive environment [2]. Two main types of corrosion are considered, i.e. pitting and general. Notably, each corrosion type will have a significant impact on the strength characteristics of different structural elements as well as on the entire structure.

The investigations of the impact of pitting corrosion on the structural capacity of different structural components can be seen in [3–8], including both experimental and numerical analyses. In the case of pitting corrosion, artificial perforation could be made without long-time corrosion development. However, when dealing with general corrosion, the only possible method to obtain the corroded samples is to corrode them in natural or accelerated conditions, as discussed in [9]. The present work deals with the problem of general corrosion. Thus, the studies discussed here only relate to this type of corrosion degradation.

Some experiments were carried out, showing the structural behaviour of different corroded structural elements. Box girders simulating the hull girder were investigated in [10–12], showing that corrosion degradation may cause a tremendous loss of structural capacity. The stiffened plates subjected to severe corrosion degradation were tested in [13], revealing that the corrosion degradation impacts the strength reduction and structural behaviour, including the post-collapse regime. Similar observations have been reached by testing other structural elements, such as beams [14]. Further numerical investigations revealed that two factors cause a structural capacity reduction. The first one is the thickness loss. The second one is related to the change of mechanical properties due to the irregularities of the corroded plate surface that are visible on a tiny scale. This phenomenon can be captured when one tests corroded plate coupons typically used to obtain mechanical properties. Such tests were performed by different studies, such as [15–19], including very thin and thick plates. One needs to be aware that the properties are slightly changed in the material scale. However, the change of constitutive material models is justified when investigating the mean stress–strain response of a typical coupon used in engineering applications.

In the work presented in [20], the FE model of stiffened plates consisting of an averaged plate thickness reduction and mechanical properties changes was developed and validated using experimental tests [13], showing a good agreement. The applicability of a similar model was proven in [14], where the flexural performance of corroded beams was investigated. The experimental studies were conducted, including the estimation of mechanical property changes as a result of the corrosion degradation development of small-scale coupons. The

* Corresponding author.
E-mail address: yordan.garbatov@tecnico.ulisboa.pt (Y. Garbatov).

https://doi.org/10.1016/j.tws.2022.110380
Received 28 January 2022; Received in revised form 2 October 2022; Accepted 17 November 2022
Available online xxxx

FE shell model consisting of coupled thickness changes together with the mechanical properties changes was adopted showing an excellent agreement with the experimental results. Apart of that, it seems that more validation work is still needed.

Only the mean value thickness reduction was considered in the model presented in [20]. However, it is observed that even when considering general corrosion, considerable scatter of the thickness distribution occurs within the single specimen [13,21]. Therefore, corrosion tests are needed to experimentally evaluate such specimens' ultimate strength [22]. However, there are time-consuming, and a limited number of samples can be obtained. Thus, efficient methods to artificially generate the field of corroded plate surfaces are needed.

Random field modelling seems to be the most suitable of various methodologies in engineering applications [23]. The examples of usage of random fields in different engineering applications can be traced in [24,25]. The possibility of applying this approach to generate the corrosion degradation distribution within the plate was explored in [26] and recently in [27]. The random fields related to corroded surfaces were applied on a small scale to obtain the mechanical properties of corroded coupons in [28,29]. The comparison between numerical calculations with experimental results [17,18] revealed an excellent agreement.

The presented study shows a novel approach to numerically modelling the structural behaviour of compressed corroded stiffened plates. Four different models are proposed, considering different thicknesses and mechanical properties modelling. The results are validated against experimental results obtained in [30], and the two-stage corrosion model is the most appropriate. The first stage modifies the general corrosion loss using measured thickness maps. In the second stage, the mechanical properties are changed to reflect the non-regularities of the corroded surface on a micro-scale based on the degradation level of a particular point of the plate surface. The resulting ultimate compressive capacity was significantly smaller, showing that the previously developed models are non-conservative. Then, the thickness distribution was modelled using a random field considering the statistical descriptors of corroded plate thickness. The numerical analyses, employing the nonlinear FE method, are performed considering different plate thicknesses and corrosion degradation levels. The results based on random fields of corrosion degradation are then compared with the deterministic solutions, and the applicability of this methodology is verified.

2. Mechanical properties of corroded plates

The changes in mechanical properties of normal strength steel were determined using experimental analysis, i.e. by testing tensile coupons subjected to marine immersed corrosion degradation. The detailed procedure and corrosion testing results were described in [22], where coupon specimens were corroded in the same conditions as stiffened plates. The specimens were made of normal strength steel of thicknesses equal to 5 mm, 6 mm and 8 mm. In general, the approach controlled only natural factors during the corrosion degradation process, i.e. temperature (by heating), water velocity (by the circulation of water) and appropriate oxygenation (by aeration).

As described in [31], the coupon specimens were tested, leading to slightly different mechanical properties changes. It must be highlighted that corrosion does not impact the steel microstructure below the level of the corroded zone. Thus, the changes in material properties are related to uneven thickness distribution within the specimen and micro pits resulting in stress concentration points. These effects affect the mean stress–strain response of the corroded specimen when subjected to tensile loading. The example of changes in mechanical properties for 6 mm plates is presented in Fig. 1. The functions of changes in mechanical properties for other thicknesses are given in [31]. The changes are presented in the function of the Degree of Degradation (DoD), which is the loss of specimen's mass considered as the fraction of the initial mass of the specimen. Notably, the presented graph points with the scatter are for the grouped results for non-corroded samples and the specimens with a low, medium and high level of corrosion degradation. For each thickness, 17 specimens in four groups were tested to achieve reliable parameters. The mean thickness loss was used to calculate the Yield stress, ultimate tensile stress and Young's modulus. Thus, if corrosion causes, ideally even thinning, no significant changes in mechanical properties will be visible. It is noted that mechanical properties are subjected to significant scatter, which is caused due to the variability in values for non-corroded material (see error bars for DoD=0%) as well as due to the complexity of the corrosion phenomenon. There are rather inherent uncertainties.

3. Finite element modelling

The stiffened plates that are the subject of current investigations are 0.4 m wide, and 1.06 m long with a stiffener of 0.1 m height, similar to specimens experimentally tested [30]. As already reported, three different thicknesses were analysed, i.e. 5 mm, 6 mm and 8 mm. The commercial software ANSYS [32] was employed to investigate the structural behaviour of corroded compressed stiffened plates.

The more advanced corrosion model considered in the study, and at the same time, close to reality, is the non-uniform degradation of the corroded surface. However, we can introduce two types of non-uniformity, i.e. global and local (see Fig. 2).

The global non-uniformity comes from the different rates of the corrosion process within the single structural element, and it is typically captured via ultrasonic measurements. The local non-uniformity, on the other hand, is very localised and cannot be captured via typical ultrasonic measurements since the observed non-uniformities (even below 1 mm) are of a lower scale than the typical size of a gauging probe. The measurement grid is also relatively scarce (Classification Societies require three measurement points per square metre [33]). Additionally, the very detailed surface cleaning and advanced scanning techniques are the only possible way, which is hard to obtain in in-situ conditions. Further, to incorporate that in the numerical model, the very dense FE mesh will be needed, leading to the considerable effort of both computations and model preparation, which is non-efficient in engineering practice. Thus, as described in the previous section, the changes in mechanical properties can capture that effect simply. To summarise, depending on the corrosion environment and process, we can get the relatively uniformly corroded element but highly non-uniform localised corrosion. From another perspective, the corrosion loss could be subjected to significant scatter, but the corroded surface can be relatively smooth. Since the mean thickness loss of the specimen is considered to calculate the mechanical properties, the corrosion model is coherent. The global thickness variation is modelled by the mean thickness loss in a larger area (the ultrasonic measurements could capture that). On the other hand, the mechanical properties are reduced to account for the localised non-uniformities leading to stress concentrations.

The SHELL181 elements were used to model both plate and the stiffener. Two types of nonlinearities are considered, i.e. geometrical and material ones. To reflect the non-linear behaviour, the static implicit solver is used, employing the Newton–Raphson iterative procedure. The material model is considered bilinear with hardening, where mechanical properties are taken as given in Section 2. The detailed information about the considered constitutive model is given in [31] and follows the equation:

$$\sigma = \begin{cases} E\varepsilon & (\varepsilon < \varepsilon_1) \\ \sigma_1 = Re_0\,(1 - 0.0061 \cdot DoD) & \left(\varepsilon = \varepsilon_1 = \frac{\sigma_1}{E}\right) \\ \sigma_1 + \frac{(\varepsilon-\varepsilon_1)(\sigma_2-\sigma_1)}{\varepsilon_2-\varepsilon_1} & (\varepsilon_1 < \varepsilon < \varepsilon_2) \\ \sigma_2 = \sigma_1 + 1.958 \cdot Re_0 \cdot \varepsilon_2^{0.154} & (\varepsilon = \varepsilon_2) \end{cases} \tag{1}$$

where ε_2 is defined in that the area under the bilinear stress–strain relationship is equal to the modulus of toughness for the particular degradation level (see [31]).

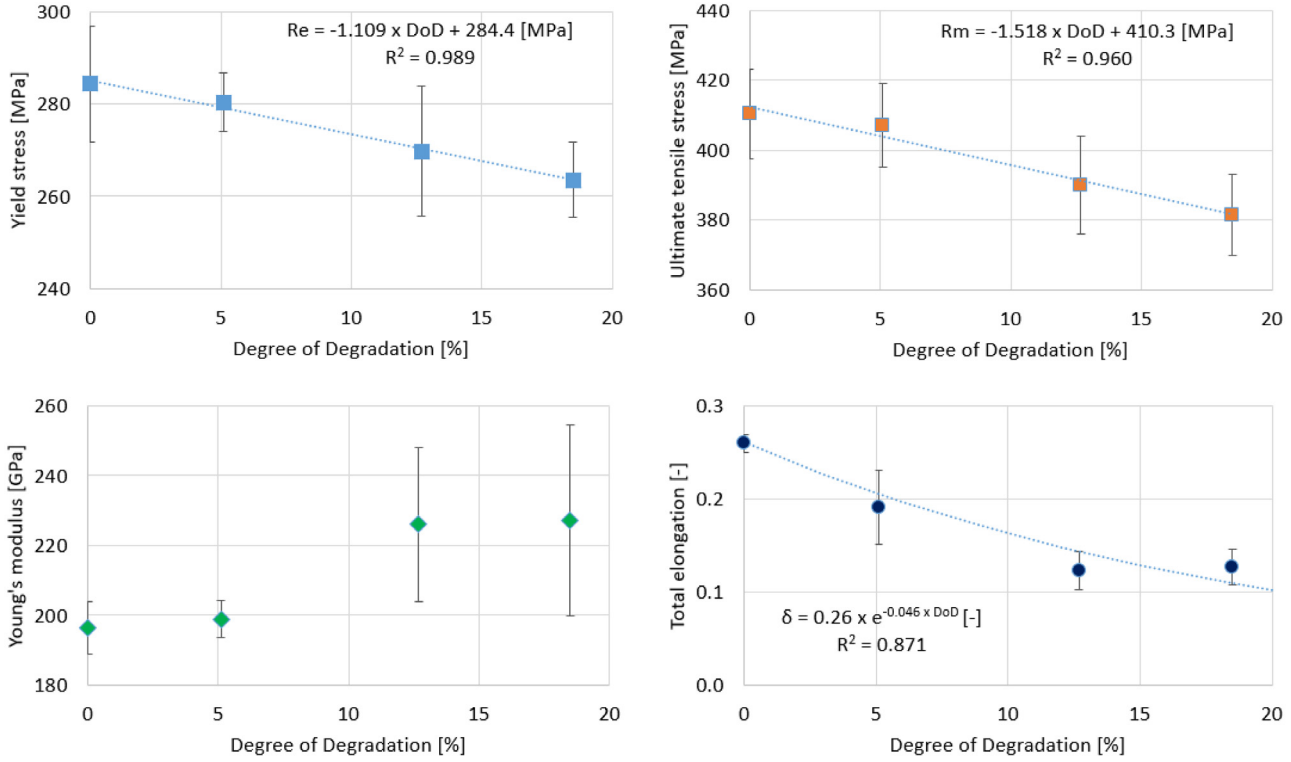

Fig. 1. Mechanical properties as a function of DoD, 6 mm specimens [31].

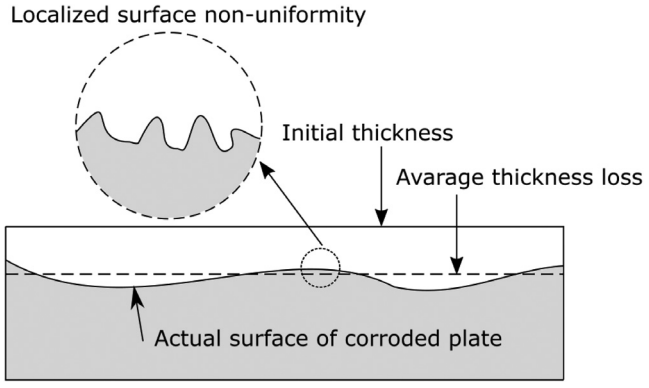

Fig. 2. Corrosion model considered in the study.

Table 1
Initial imperfections of corroded stiffened plates [34].

Thickness [mm]	DoD [%]	a_1 [mm]	a_2 [mm]	b_1 [mm]	b_2 [mm]	c_0 [mm]
5	0	2.78	3.37	−6.98	4.49	2.95
	7	2.37	5.19	−7.98	5.37	1.19
	14	2.33	3.49	−5.34	3.95	0.00
	21	3.45	3.05	−8.91	9.02	3.35
6	0	4.01	4.17	3.58	−4.95	0.72
	7	4.36	3.21	0.63	−5.19	0.60
	14	3.73	3.66	3.69	−4.10	2.18
	21	4.62	3.12	2.19	−5.01	0.85
8	0	4.61	5.05	−1.01	−1.07	0.45
	7	4.31	5.07	−0.25	−0.11	0.44
	14	3.77	5.50	−3.01	−2.43	0.22
	22	4.25	4.73	1.39	1.46	0.77

The mesh convergence studies have been performed, showing that the element size of 0.02 m will result in the excellent prediction of the structural response and will provide relatively low computational time. In Fig. 3 (left), the applied boundary conditions are presented as similar to the experimental ones. Thus, the loaded edges of the plate and the stiffener are clamped, whereas unloaded edges are left free. The experimental stand with the placed specimen is presented in Fig. 3 (right). A specially designed clamping system was used to achieve the clamped boundary conditions. Initial imperfections based on the photogrammetry measurements were incorporated into the FE model for the deterministic analysis. Detailed information about photogrammetry measurements is given in [34], and the generic shape of imperfections is presented in Fig. 4. The values of considered imperfections are introduced in Table 1, where symbols are regarding Fig. 4. The welding-induced distortions are applied by changing the z-coordinate on each node of the plate element.

To model the corrosion degradation, the thickness at each finite element node is changed based on the measured thickness distribution (see an example of the thickness map in Fig. 5). Then, the local degradation level of the element is calculated based on the mean value of the thickness in four nodes. Furtherly, the mechanical properties of a particular element are changed based on the local degradation level according to the constitutive models as presented in Section 2.

4. Deterministic approach

4.1. Comparison between different corrosion models

Before the detailed comparison between numerical and experimental results, the hypothesis that non-uniform thickness loss and local changes of mechanical properties are the reason for the impact of corrosion on the structural behaviour of corroded compressed stiffened plates is verified. Thus, four different corrosion models are compared with experimental results:

- non-uniform thickness loss with subsequent mechanical properties;

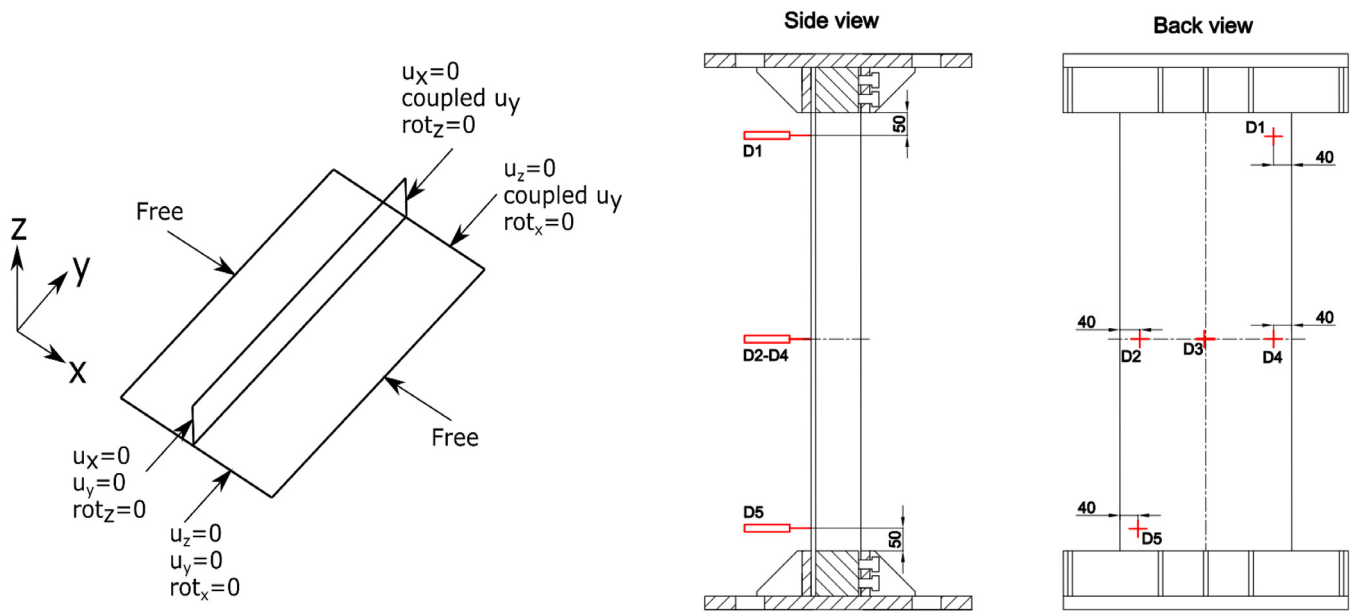

Fig. 3. Applied boundary conditions of the modelled stiffened plate (left) and experimental stand with the placed specimen (right).

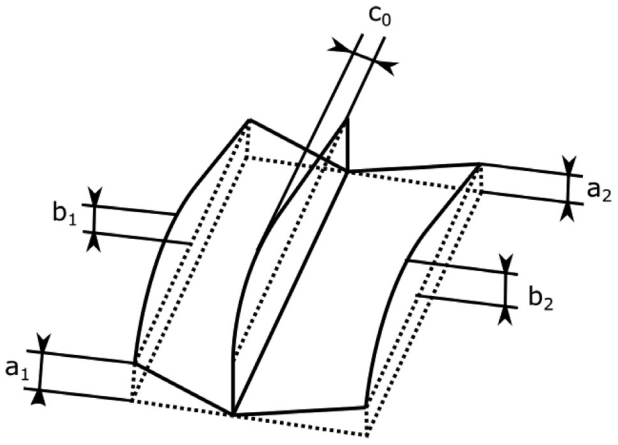

Fig. 4. Initial imperfections [34].

- non-uniform thickness loss without changes in mechanical properties;
- uniform thickness loss with subsequent mechanical properties reduction;
- only uniform thickness loss.

The corrosion degradation level, measured as the percentage loss of the material, was obtained equal to approx. 7%, 14% and 21% for each of the initial thickness of the plate. For each model, the ultimate strength values are plotted in function of degradation level. The comparison for 5 mm plates is presented in Fig. 6. It is noted that the closest results to the experimental ones were observed for the model with non-uniform thickness reduction and subsequent reduction of mechanical properties. Although some bias is observed, the inclinations of regression curves are almost the same. The bias between experimental and numerical results is also observed for the intact specimen. The possible causes of this bias could be the non-ideal capturing of natural boundary conditions in the numerical model and uncertainties in capturing mechanical properties and initial imperfections. The detailed analysis of lateral plate deflections near the supports and comparison with the FE analyses with both clamped and simply supported boundary conditions revealed that fully-clamped conditions were not achieved [35]. Several possible reasons were identified, including the non-ideal force transition via the testing machine, the possible eccentricity of axial loading, and the unfairness of both stiffened plate and supporting structure. It was concluded that the total restriction of the plate rotation is challenging in experimental conditions, leading to the possible creation of plastic hinges. Since there are complex phenomena, the differences between experimental and numerical results could be different depending on the initial thickness of the samples. The highest values of the ultimate strength are observed when only the mean thickness reduction is considered. The specimens with non-uniform distribution of the thickness also showed lower results when compared to a uniform model. Fig. 7 compares different models for 6 mm stiffened plates. It is noted that a very good match has been achieved between experimental results and the most sophisticated numerical model. All other models overestimated the values of ultimate strength. Notably, better results were achieved, where non-uniform thickness distribution was applied only compared to a uniform model with subsequent reduction of mechanical properties. This indicates the crucial role of the actual distribution of thickness in the stiffened plate. The comparison of the results obtained for different models for 8 mm specimens is presented in Fig. 8. Similarly to other thicknesses, the closest results to experimental ones were obtained for the model that considers the accurate thickness distribution and changes in mechanical properties. The inclination of both curves is the same; however, slight bias is observed for the non-corroded specimen. It is noted that concerning other models, close results were also obtained for a model that considers uniform thickness loss and reduction of mechanical properties. Where non-uniform thickness loss is considered only, the results are away from the experiment. Thus, it was more crucial to consider the mechanical properties reduction rather than the actual thickness distribution in this case. This analysis shows that the results are closest to the experiment when considering both uneven thickness distribution and mechanical properties changes. This indicates that when the model considers only the uniform thickness loss, not solely the ultimate strength will be overestimated, but the post-collapse form will not be captured accurately. For some stiffened plates, the more crucial was taking into account the changes in mechanical properties, whereas for others, the proper modelling of thickness distribution. However, only considering these factors simultaneously will allow capturing the corroded compressed stiffened plate's behaviour most accurately. Thus, this model is chosen for further investigations.

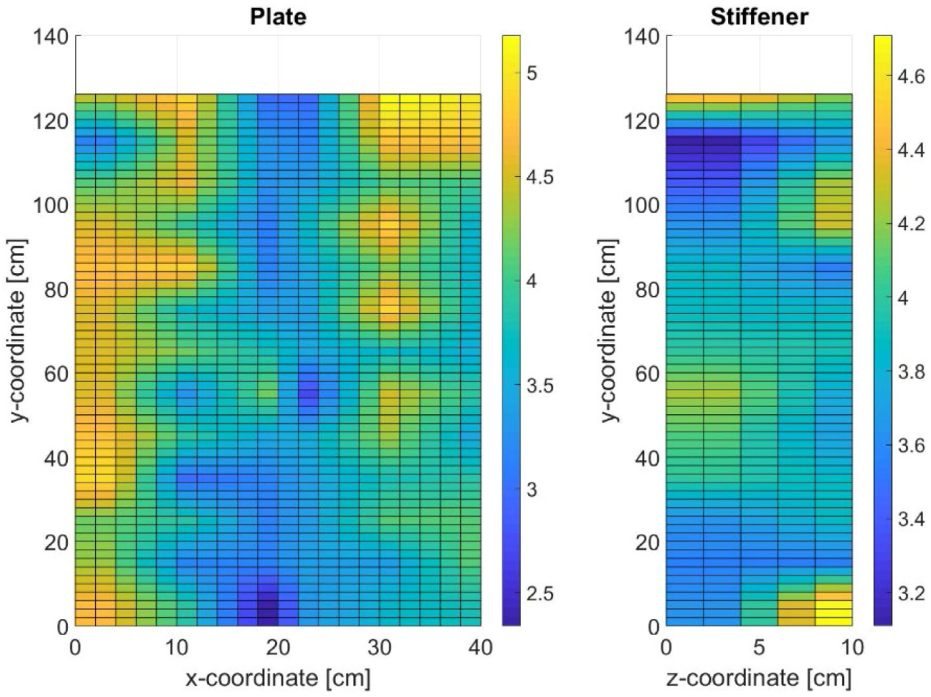

Fig. 5. Example of thickness distribution within specimen in mm, 5 mm stiffened plate, DoD = 21% [22].

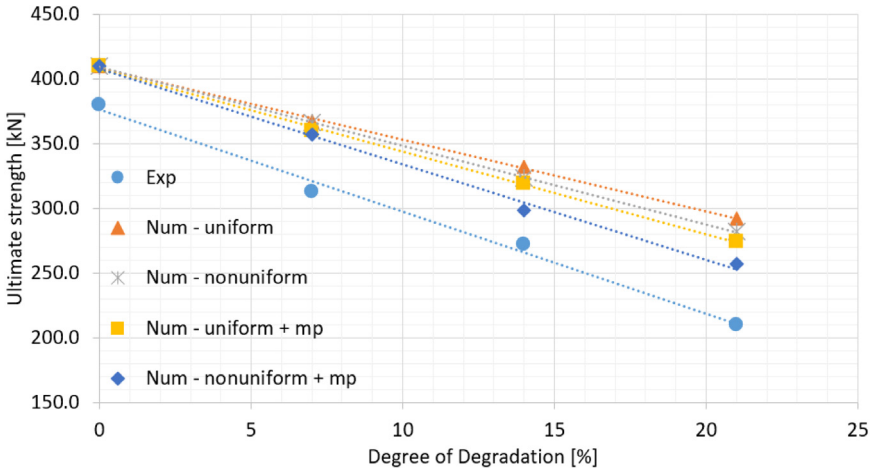

Fig. 6. Comparison between different corrosion models, 5 mm stiffened plates.

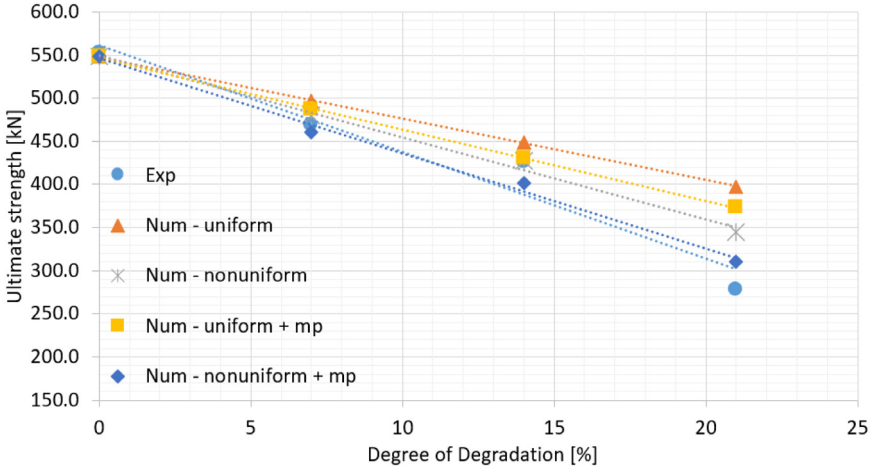

Fig. 7. Different corrosion models, 6 mm stiffened plates.

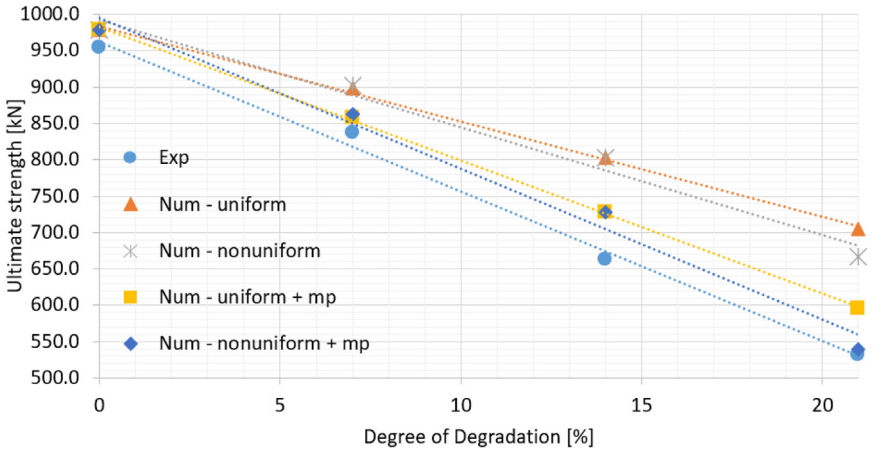

Fig. 8. Different corrosion models, 8 mm stiffened plates.

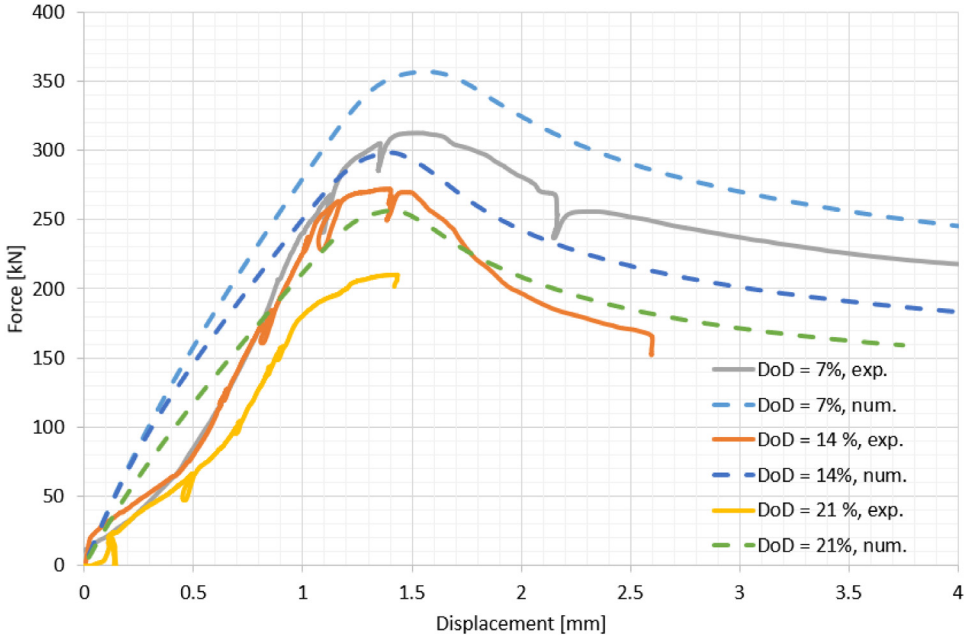

Fig. 9. Force–displacement relationships for 5 mm specimens.

4.2. Detailed validation of numerical model

Firstly, the force–displacement curves are adjusted, leading to the ultimate point being observed for the same longitudinal displacement. The comparison between numerical and experimental results for 5 mm plates is presented in Fig. 9. All cases generally have an observed bias between numerical and experimental results. A similar difference has been observed for an intact case, and possible reasons were discussed in the previous section. However, the curves are pretty similar in terms of pre-and post-collapse behaviour. It is noted that the initial inclination of curves is significantly lower in the case of an experiment, and after crossing 0.5 mm of displacement, the inclinations are similar to numerical predictions. The comparison between the numerical and experimental results for 6 mm plates is presented in Fig. 10. In the case of ultimate strength, the higher values are observed for the experiment in 7% and 14% of degradation level, whereas the lower value is observed for 21% of DoD. The force–displacement path is almost identical between the experiment and numerical predictions for the specimen with the lowest corrosion diminution. In other specimens, the initial slope of the experimental curves is shallow due to fixing the specimens in the supports. However, apart from that, pre-collapse behaviour is somewhat similar. The significant differences after the collapse are observed only for the specimen with a medium level of corrosion severity. The comparison between numerical and experimental results for 8 mm plates is presented in Fig. 11. It is noted that in the case of 7% and 21% degradation levels, the ultimate strength is almost the same in the case of experimental and numerical results. However, some difference has been obtained for a degradation level of 14%. In pre-and post-collapse behaviour, the curves are very similar for 14% of DoD. For 21% of DoD, before reaching the ultimate point, the experimental and numerical path is very similar, whereas post-collapse behaviour is more dramatic for a numerical one. The most visible differences are observed for a degradation level of 7% within the entire force–displacement relationship. The comparison of lateral displacements in the mid-cross section between experimental and numerical results is presented in Fig. 12 regarding 5 mm specimens. The displacement gauge's positions are presented in Fig. 3 (right). It is noted that excellent convergence has been obtained between the FE model and experiment. In each case, the displacements in both sides of the stiffener (ud2 and ud4) increased in the opposite direction, indicating local plate bending from the beginning of the loading process. Simultaneously, the lateral mid-displacement (ud3) was close to zero, indicating that local plate

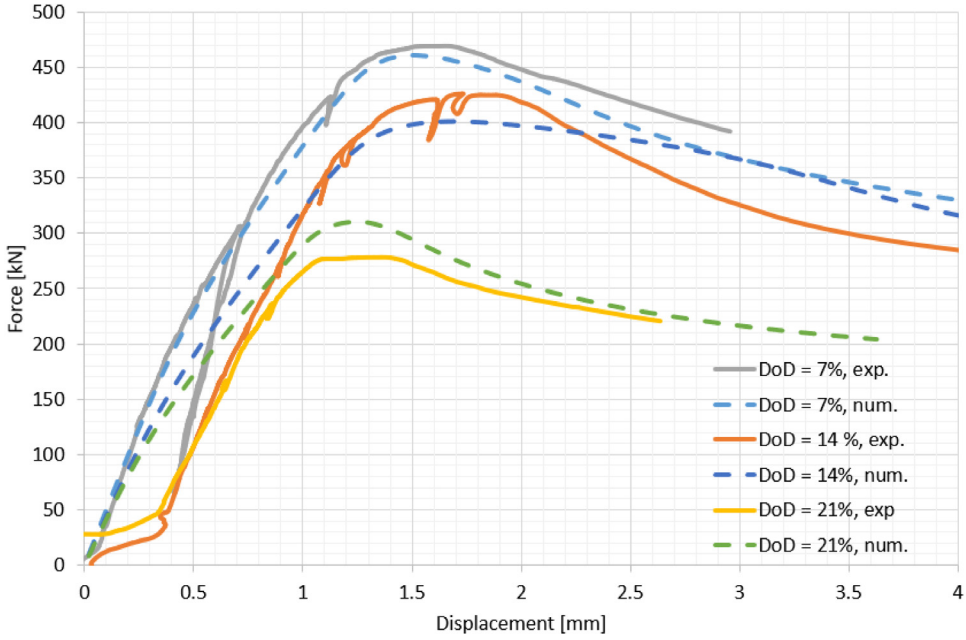

Fig. 10. Force–displacement relationships for 6 mm specimens.

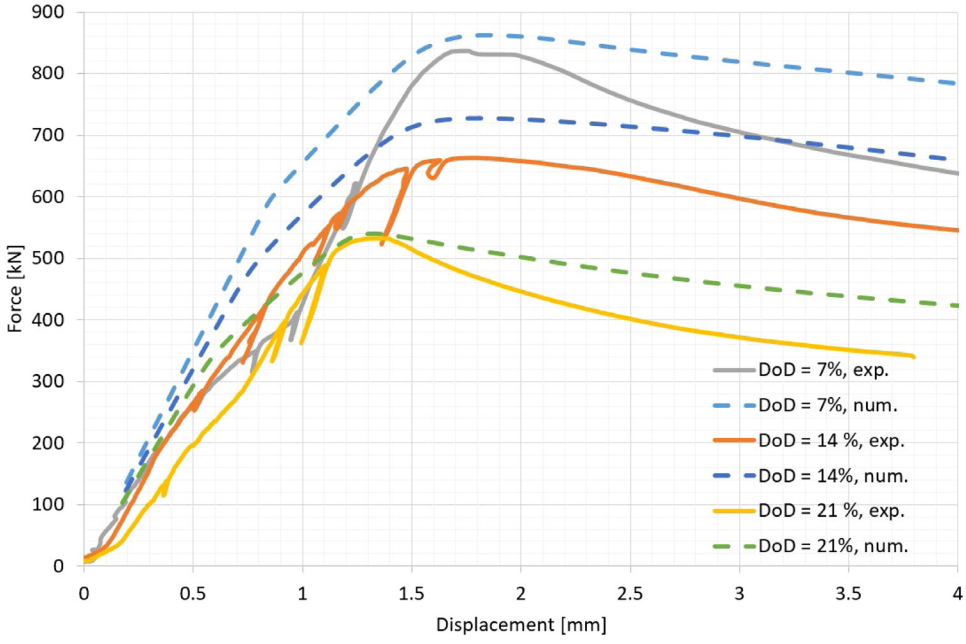

Fig. 11. Force–displacement relationships for 8 mm specimens.

buckling and stiffener tripping were the dominant failure modes. The only significant displacements in the connection of the plate and the stiffener were noted in a specimen with a 14% of degradation level. However, it was captured only in an experimental domain. For all cases, the lateral displacements increased when ultimate capacity was reached and stayed constant after crossing that point. Fig. 13 shows the lateral displacements for 6 mm specimens. It is observed that for DoD equal to 7% and 14%, the experimental readings and numerical predictions are similar. However, higher displacement values are noted in the case of an experiment. In these cases, the readings increased up to the level of ultimate strength value and then stabilised at a constant level. This indicates that the plate-induced buckling was the leading cause of the collapse. However, for a specimen with a degradation level of 7%, some global buckling occurred too in a tested specimen, which is noted in slightly increasing lateral mid-displacement. This was not observed in the FE model. In the case of a most severely corroded specimen, the global collapse mode has been observed in an experiment. The lateral displacements after collapse increased significantly in the same direction. However, the numerical model predicted another failure mode, similarly to previous specimens. Fig. 14 shows the lateral displacements obtained for 8 mm specimens. It is noted that there was no local plate bending at the beginning of the loading process, and all displacements were very close to zero. However, with the corrosion development, the plate on both sides of the stiffener starts to buckle faster, and this was observed for both numerical and experimental investigations. This observation is easily understandable since with the increase of the corrosion level, the mean plate thickness decreases and the slenderness ratio increases. Thus, the plate is more prone to

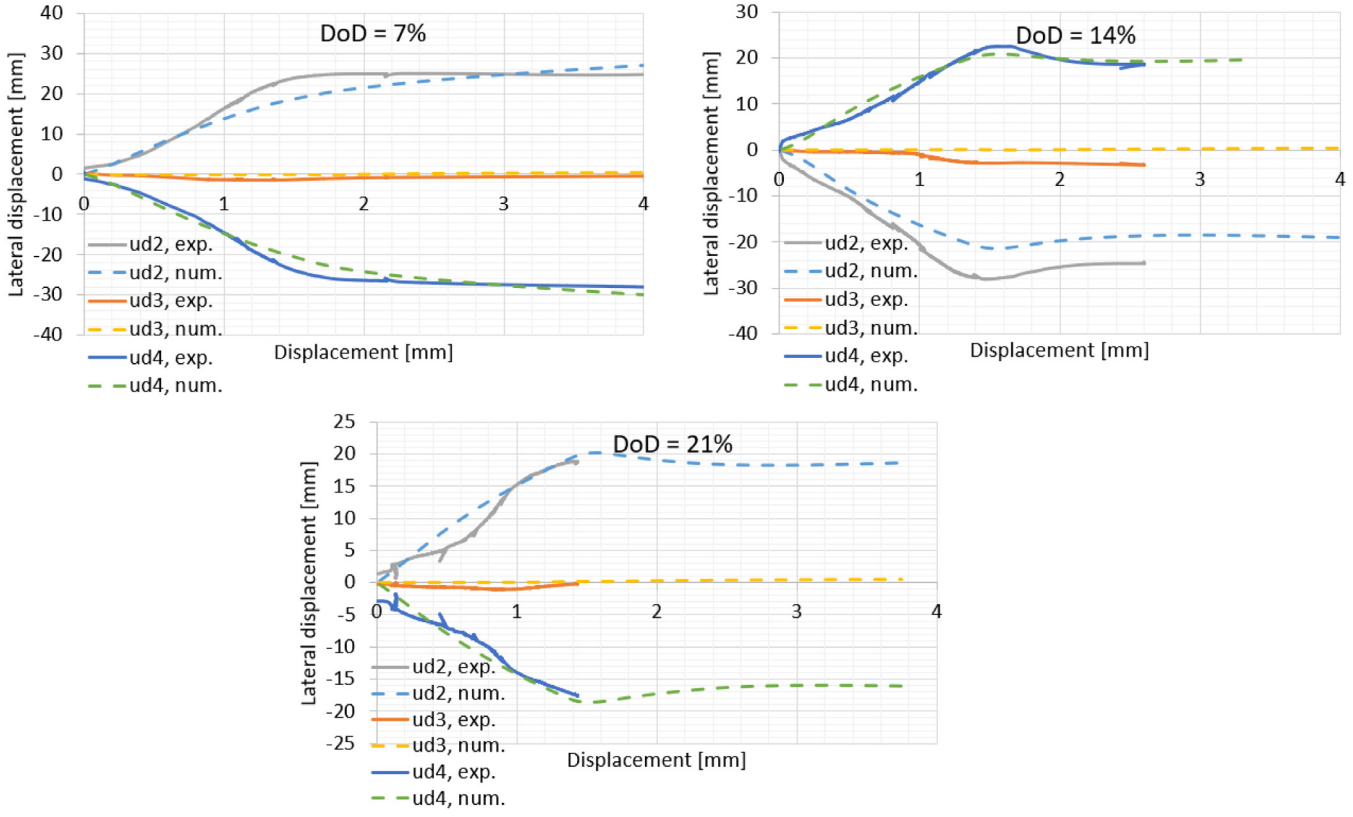

Fig. 12. Comparison of lateral displacements, 5 mm specimens.

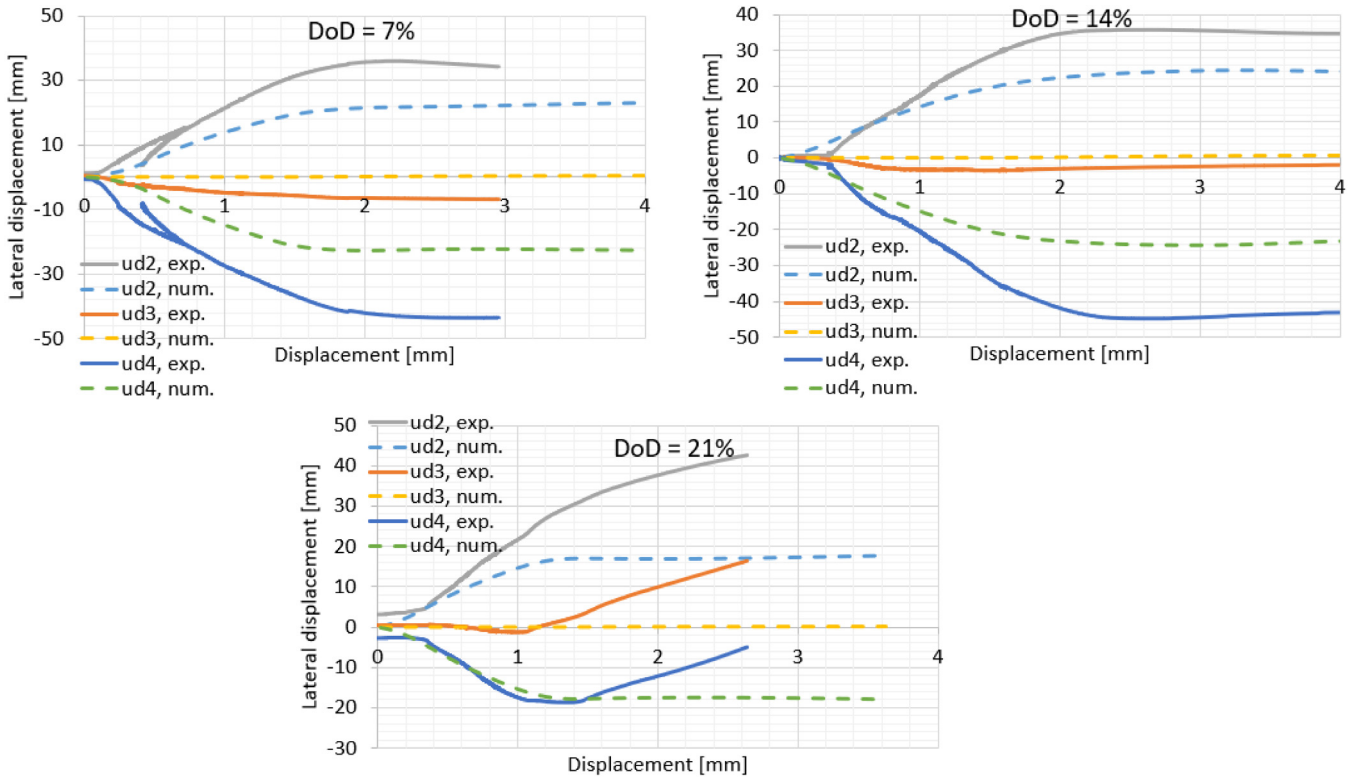

Fig. 13. Lateral displacements, 6 mm specimens.

buckle. For the specimen with a level of degradation of 21%, the plate is subjected to local bending almost from the beginning, similarly to stiffened plates of lower thickness values (5 mm and 6 mm).

Nevertheless, the buckling moment is slightly different for the FE model and tested specimens considering 14% and 21% of the degradation levels. In terms of lateral mid-displacement (ud3), some differences

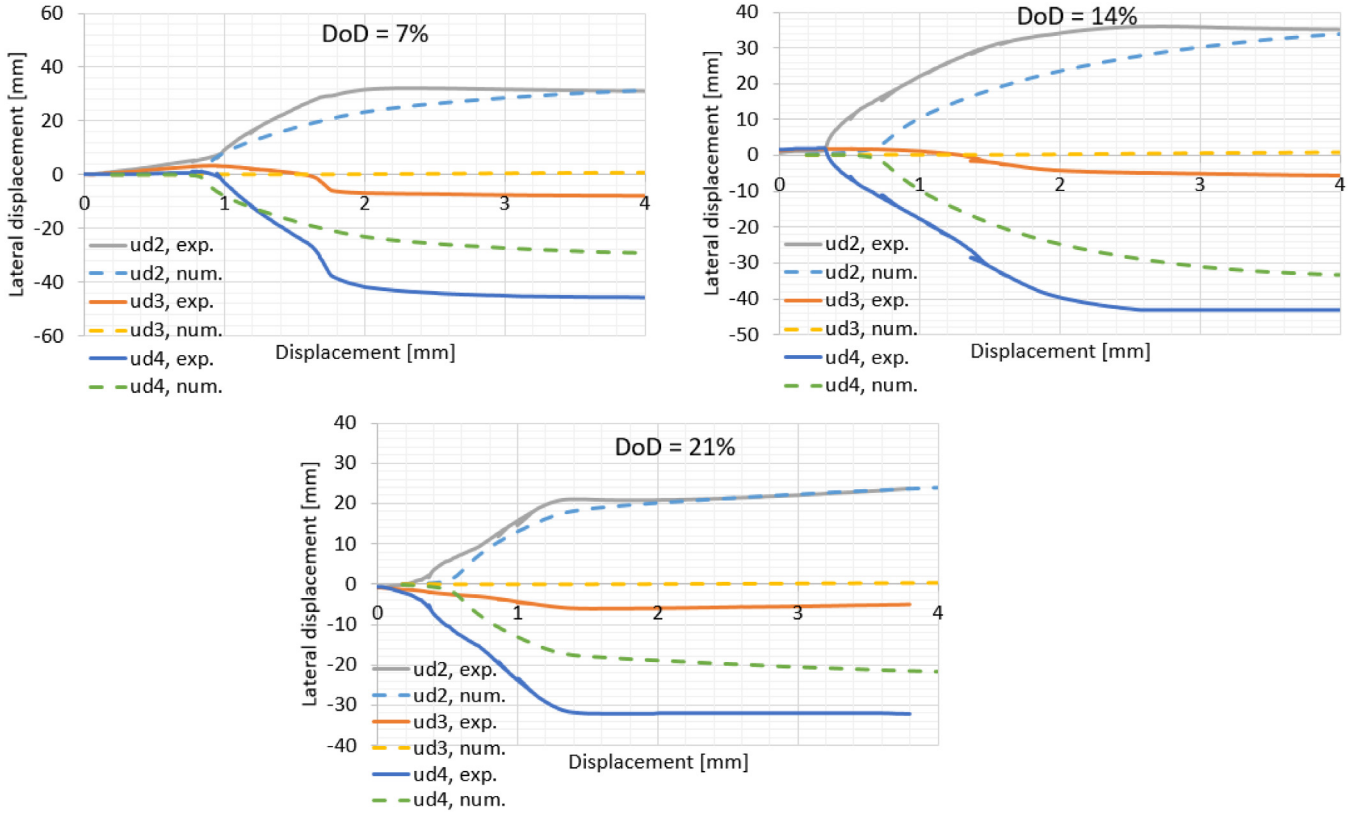

Fig. 14. Lateral displacements, 8 mm specimens.

could be noted too. In the case of the experiment, some level of global bending occurred during failure, which was not captured in the FE model. Although the experimental displacements are slightly higher than the numerical ones, it could be concluded that a very good match has been achieved. Finally, the post-collapse shapes of tested specimens [30] are compared with the results of the FE analysis. The failure modes from FE analysis for 5 mm specimens are presented in Fig. 15. Similarly to the tested specimens, the post-collapse forms are unsymmetrical and not observed when thickness distribution is uniform. The primary cause of the collapse is identical for both the experiment and numerical model, i.e. local plate buckling followed by stiffener tripping. It is noted that only in a specimen with a 14% degradation level the post-collapse forms are almost identical. In a specimen with a 7% degradation level, the region with the highest plastic deformations is closer to the upper support. For the specimen with a 21% level of degradation, the critical cross-section is on the opposite side compared to the experiment. The possible cause of differences could be the non-ideal capturing of an actual thickness distribution due to the uncertainty of the measuring technique. Secondly, the uncertainty in capturing the distribution of mechanical properties could be the reason.

Fig. 16 presents the post-collapse shapes of 6 mm specimens obtained via the numerical tool. Compared with failure modes observed in tested specimens, almost identical forms were observed for specimens with DoD levels of 7% and 14%. Thus, the local plate buckling followed by stiffener tripping caused the collapse, and the highest deformations were noted near the lower support. However, in the most severely corroded stiffened plate, the global buckling was primarily visible in a tested specimen, which was not captured in a numerical model. Nevertheless, both cases observed local plate buckling near the upper support.

Fig. 17 shows the failure modes of the 8 mm specimens from numerical analysis. It is noted that the post-collapse shapes are similar and unsymmetrical. In all cases, the local plate buckling was a primary cause of the collapse, which was also observed experimentally. However, in the latter case, some global buckling was also observed. Nevertheless, the shapes of collapsed plates, including critical cross-sections, were almost identical to those observed in tested specimens. In all cases, the highest plastic deformations occurred near the lower support.

The presented comparison shows that the FE model, which includes real thickness distribution and changes in mechanical properties, correctly simulates corroded stiffened plates' behaviour. As a result of the FE estimations, the achieved ultimate strength was very close to the experimental one. Only for 5 mm specimens, some bias in the ultimate strength value was observed. However, for all thicknesses, there were notable differences between both force–displacement curves and failure modes. The first possible reason is related to the non-ideal clamped boundary conditions in the experimental testing, which was already discussed in Section 4.1. This could be the reason behind the differences in the initial inclination of the force–displacement curves (fixing of the specimens in the supports) and differences in post-collapse shapes (e.g. positions of the cross-section with highest deflections). The upper and lower support could act slightly differently, especially since the upper support was subjected to hydraulic pressure. However, as found in [35], both the upper and lower cross-sections of the specimen are restrained from out of plate rotation, and the shape of the stiffened plate resulted in solid support. It was concluded that the clamped boundary conditions, as defined in the present study, have been achieved in restraining the stiffened plate cross-sections from rotation in the supports. Although some local rotation of plating was observed, applying a special supporting system has minimised the gap between the support and specimen.

Further, the upper and lower supports could not ideally be in the same line due to manufacturing tolerance, leading to initial eccentricity not modelled in the FE code. The thickness distribution of specimens could also be different due to the uncertainty of the measuring technique. This could lead to a difference between real thickness distribution and those modelled numerically; consequently,

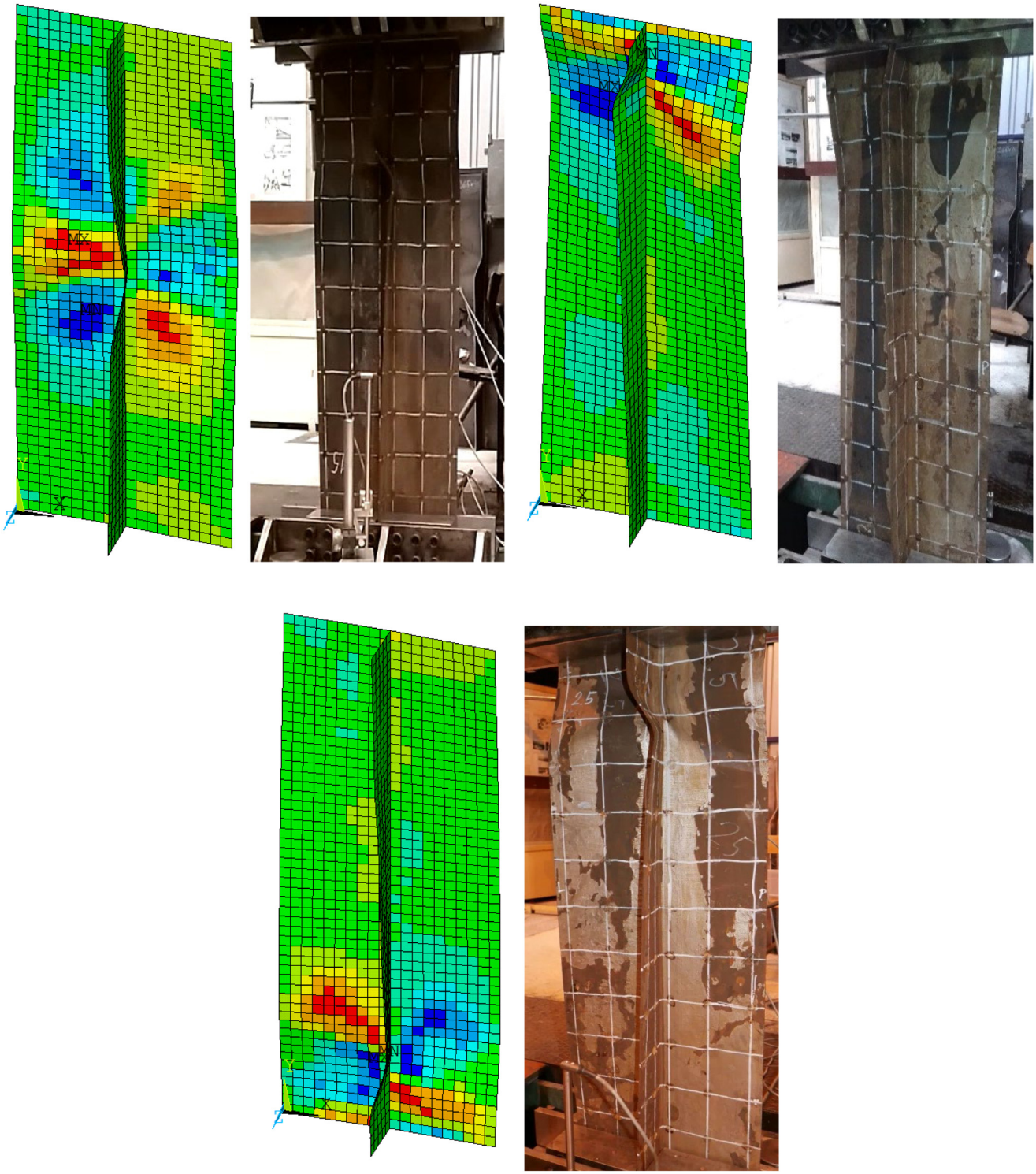

Fig. 15. Post-collapse shapes, 5 mm specimens (DoD = 7% - left, top, DoD = 14% - right, top, DoD = 21% - bottom).

a post-collapse form could be slightly different. Finally, as noted in Fig. 2, the mechanical properties are subjected to scatter even for non-corroded samples. This could lead to the different spatial distribution of mechanical properties in a tested sample compared to the numerical model. This would have an impact on both the force–displacement relationship and failure mode. Although there were various uncertainty sources, in almost all cases, the force–displacement relationships, lateral displacements and post-collapse forms generally agreed between the numerical model and experiment.

5. Random field approach

5.1. Modelling

Due to the complexity of methods for measurements of different structural imperfections, such as corrosion degradation, initial distortions, etc., random field modelling [23] seems to be a powerful tool for such imperfections. The spatial distribution of irregularities of the corroded surface may be modelled by the random field approach as the

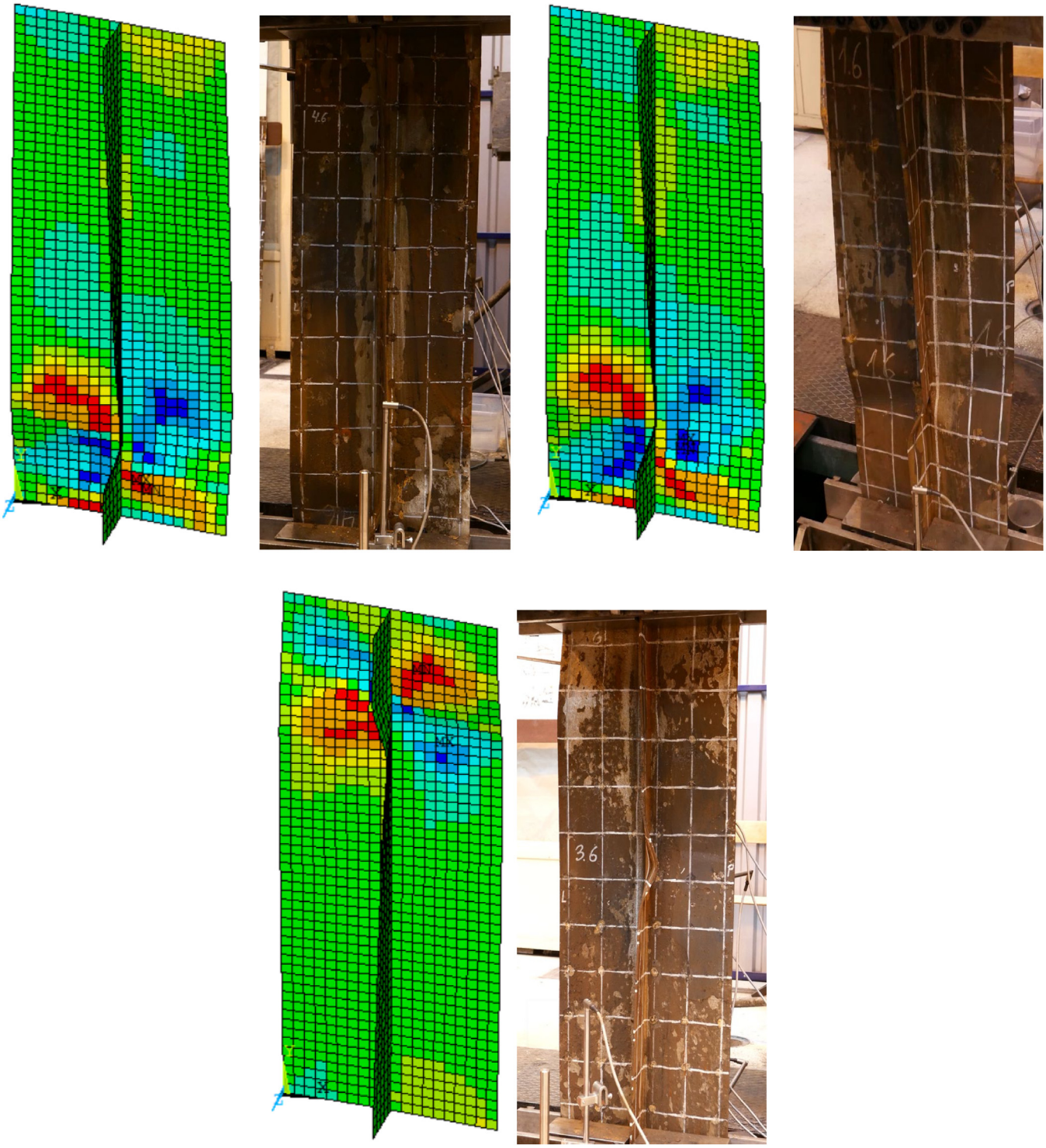

Fig. 16. Post-collapse shapes, 6 mm specimens (DoD = 7% - left, top, DoD = 14% - right, top, DoD = 21% - bottom).

one that is the most suitable for this purpose due to the set of an infinite number of spatially correlated random variables. Thus, for engineering applications, the discretisation technique needs to be applied to be suitable as an input for numerical modelling, e.g. the FE method. Different discretisation methods exist, and pieces of information can be easily found in different sources, e.g. [36,37]. The Karhunen–Loeave expansion [36] is employed in the presented work, and the Gaussian random field is considered. The field is assumed to be homogeneous and stationary, and it is fully described by its mean value $\mu(\boldsymbol{x})$, variance $\sigma^2(\boldsymbol{x})$ and autocovariance function $C(\boldsymbol{x}, \boldsymbol{x}')$. There are different types of auto covariance functions and the exponential one is used in the present study:

$$C\left(\boldsymbol{x}, \boldsymbol{x}'\right) = \exp\left(\frac{(\boldsymbol{x}-\boldsymbol{x}')^2}{x_0^2}\right) \tag{2}$$

where $(\boldsymbol{x} - \boldsymbol{x}')$ is the absolute distance between any two points in the meshed corroded plate surface and x_0 is the correlation length.

The correlation length is the parameter that primarily governs the spatial variation of the random field. When the correlation length is higher, the field is strongly correlated and becomes smooth. Similarly,

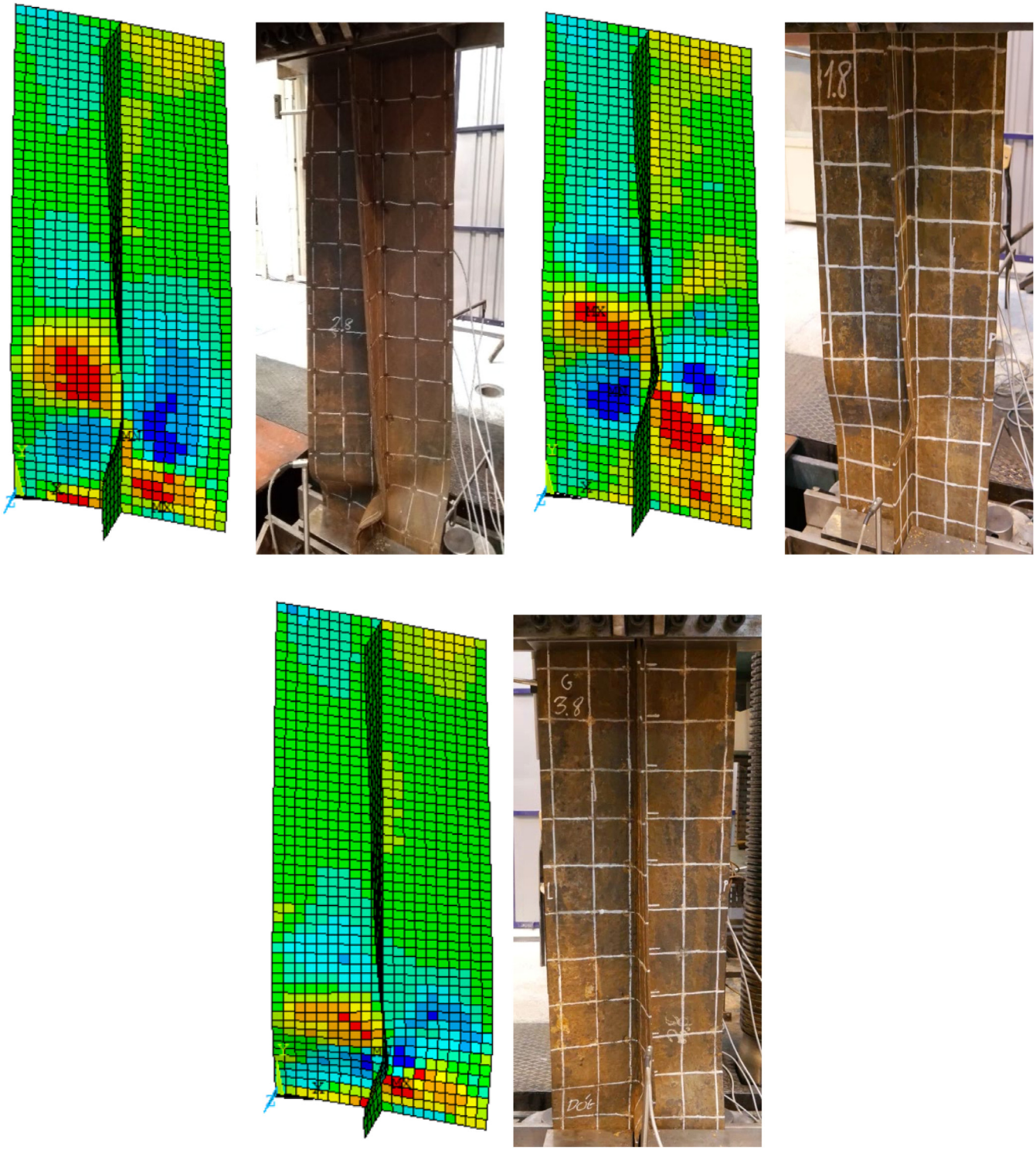

Fig. 17. Post-collapse shapes, 8 mm specimens (DoD = 7% - left, top, DoD = 14% - right, top, DoD = 21% - bottom).

with the decrease in the correlation length, the field is only slightly correlated, and the surface is more irregular than the highly correlated field. The fields representing different levels of correlation are presented as an example in Fig. 19.

To generate the random field for the specific mesh and with different statistical characteristics (standard deviation, correlation length), the MatLab software [38] is used, employing a specially developed code [39]. The random field's standard deviation is taken as presented in Table 2, which was taken based on the measurements carried out in corroded stiffened plates [22]. The correlation length and standard deviation of the corrosion fields are considered identical for the plate and the stiffener when considering a single stiffened plate. Similarly, the mean thickness loss is also the same in both plates and the stiffener for the particular value of DoD. Further, the random fields in the plate and stiffener were generated separately. For generated thickness distribution, the mechanical properties will vary depending on the corrosion degradation of any particular finite element. Thus, the approach is similar to the deterministic analysis presented in Section 3. The changes in mechanical properties were also based on the experimental results described in Section 2 and differed depending on the initial thickness.

Table 2
Statistical descriptors of residual corroded plate thicknesses.

DoD [%]	Initial thickness [mm]	Corrosion depth [mm]	
		Mean value	Standard deviation
10.5	5	0	0.251
21	5	0.525	0.419
10.5	6	1.05	0.587
21	6	0	0.251
10.5	8	0.63	0.452
21	8	1.26	0.654

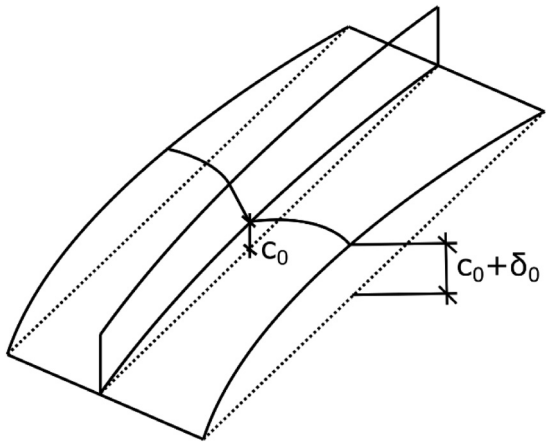

Fig. 18. The model of initial imperfections used for the random approach.

Since, in the case of the random approach, a higher number of cases is analysed with regards to the deterministic approach, the level of initial imperfections is assumed to be constant for specific plate slenderness, leading to the same shape of imperfections for the particular plate thickness. Thus, the effect of corrosion could be captured without the uncertainty related to different imperfection shapes within considered cases. The model suggested by Smith [40] and further explained in [41] is adopted to model the welding-induced initial imperfections. The imperfections are modelled as a superposition of global column imperfections c_0 and local plate imperfections δ_0 (see Fig. 18). The local plate distortions are a function of plate slenderness ratio β:

$$\beta = \frac{w}{t}\sqrt{\frac{Re}{E}} \tag{3}$$

where w is the plate width, and t is the plate thickness. The average level of local plate imperfections is considered as $0.1\beta t^2$. The global column imperfections are taken as $0.0015\ l$, where l is the length of the stiffened plate. The sideways stiffener imperfections were modelled as well, with the amplitude equal to c_0.

5.2. Sensitivity studies

A sensitivity analysis is performed to investigate the impact of a random field's governing characteristics. The stiffened plate of a 6 mm thickness and with $DoD = 21\%$ is chosen to analyse the influence of the parameter variations on the resulting ultimate compressive strength. Two different characteristics of the random field are considered: correlation length and standard deviation. Additionally, the convergence studies were performed to see how many random field realisations concerning one case are enough to provide a stable mean value.

The correlation length was investigated between 7 mm and 316 mm. The minimum level is related to the mesh discretisation since the correlation highly below the element size will not be traced, and the thickness of the following two nodes will not be correlated. On the other hand, the corrosion depth changes above a certain correlation length level cannot be more distinguished. Thus, the maximum applicable correlation length was estimated at 316 mm. The examples of random fields with different levels of correlation considering both the plate and the stiffener are presented in Fig. 19. It needs to be noted that the random fields for the plate and stiffener are generated separately.

The random field methodology is advantageous. However, it requires a specific number of realisations. Although the two random fields of corrosion degradation, considering both the plate and the stiffener, will have identical statistical characteristics (correlation length and standard deviation), the resulting compressive ultimate strength of stiffened plate may be different. Thus, instead of one specific realisation, the mean value from several of them will be much more representative. The so-called convergence studies are performed to find the proper number of realisations that will result in a stable mean value. The analysis is performed for a correlation length of 0.1 m. With the increase in the number of realisations, the mean value is calculated as:

$$\overline{x_n} = \sum_{i=1}^{n} \frac{x_i}{n} \tag{4}$$

where n is the number of realisations and x_i is the ultimate compressive strength for a specific realisation. Fig. 20 shows the mean value of the ultimate strength considering an increasing number of realisations. It can be noticed that three realisations start to provide a stable mean value. Within the range between 3 and 9 realisations, the mean value changes within the margin of ±1%, which could be considered a tiny error in that type of computation. Nevertheless, for better convergence, nine cases are considered in further studies. The ultimate normalised strength as a function of the correlation length is presented in Fig. 21, which is estimated as the ultimate force divided by cross-sectional area and yield stress. The normalised capacity is calculated always considering the initial values of the thickness and yield stress, even when corroded specimens are evaluated. For each correlation length, the box and whiskers plot is presented.

It is noticed that when the corrosion fields are more correlated, the reduction of ultimate strength is more significant. Within the range of the correlation length between 0.1 m up to 0.316 m, the mean value of ultimate strength is quite similar. Additionally, for a lower correlation length, the scatter of the resulting ultimate capacity is lower. The most critical case appeared to be for the correlation length of 0.1 m, which results in a minimum mean value. However, the most critical case was captured within the highest correlation value in terms of a single realisation. Finally, it is noticed that the ultimate strength of corroded stiffened plates is subjected to relatively high uncertainty. The maximum and minimum point difference within all realisations reaches 20% of the mean value. The resulting ultimate strength is governed not only by the degradation level, but the thickness distribution within the specimen is an essential parameter that changes the structural behaviour, which was also observed for the deterministic approach.

In the case of a lower correlation length, the areas of high corrosion diminutions will be smaller compared to a more extended correlation, which can be observed in Fig. 19. This leads to a different structural response. Actually, with a very high correlation, even the entire cross-section may have a smaller thickness concerning the mean value of corrosion degradation, leading to the premature collapse of the entire specimen.

This phenomenon can also be captured when one compares the post-collapse shapes, as presented in Fig. 22, for some selected cases of different correlation lengths. It is distinguishable that the position of the collapsed cross-section is quite different. In the case of higher correlation, the collapse may be very close to the loaded edges if the region of the reduced thickness occurs in that place. Nevertheless, the failure mode is quite similar for all cases, and it is caused by the local plate buckling followed by stiffener tripping. The differences will also occur when comparing the force–displacement curves.

The standard deviation of the random field is assumed based on the measurements, as presented in Table 2. However, the actual scatter of the plate thickness may be different in some cases, depending on

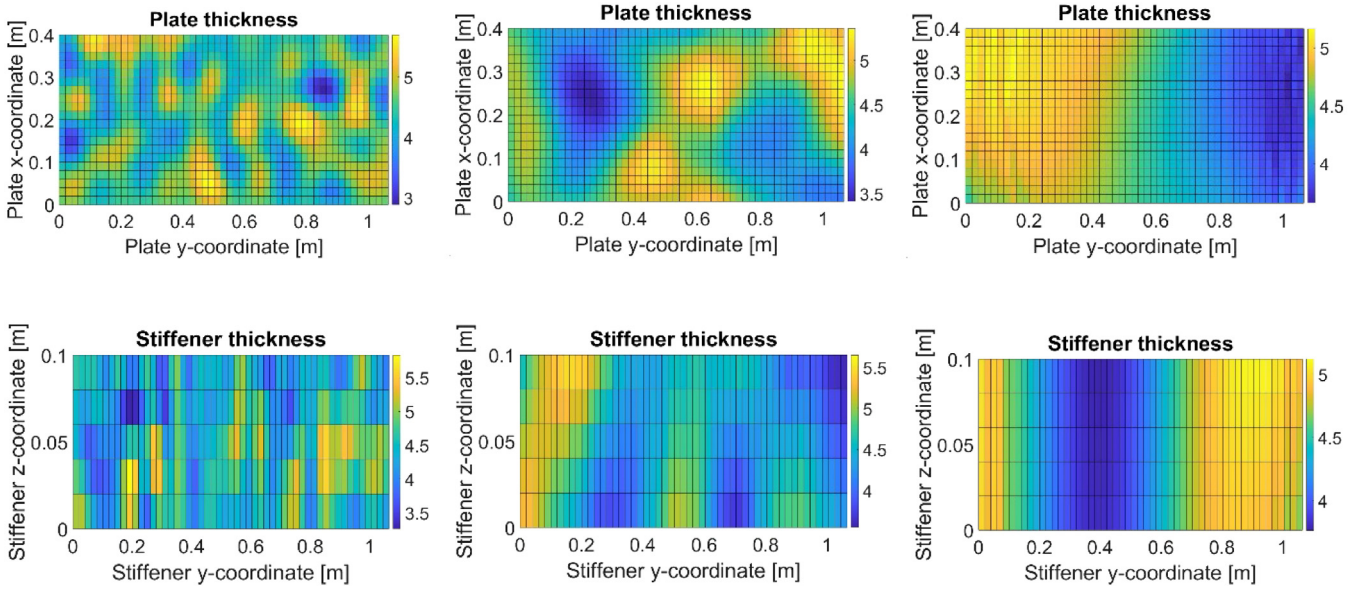

Fig. 19. Random fields of corroded plates and stiffeners with low (left), moderate (mid) and high (right) correlation.

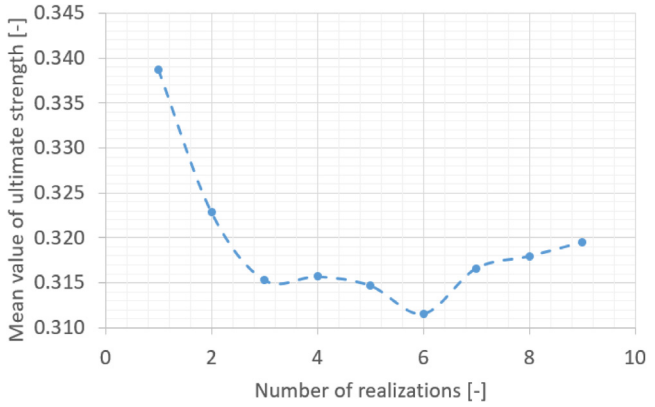

Fig. 20. Convergence studies concerning realisations number (correlation length of 0.1 m).

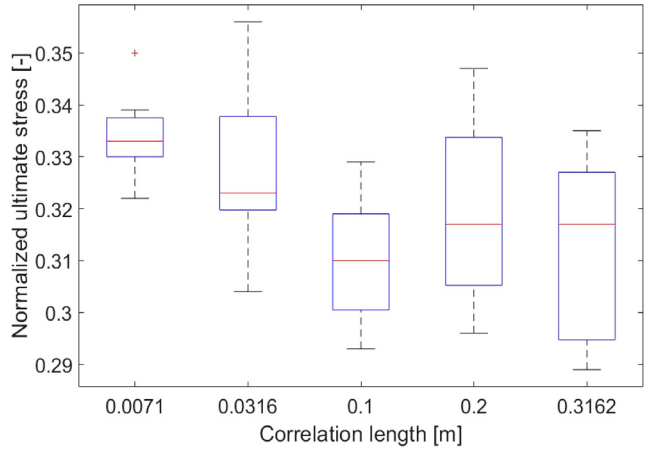

Fig. 21. Box and whiskers plot of normalised ultimate strength.

the corrosion environment [42]. Thus, the thickness standard deviation level is investigated to see the possible impact on the ultimate strength reduction. In each case of correlation length, the representative random field providing ultimate strength closest to the mean value from nine realisations was taken into account. Two standard deviation levels were investigated for each correlation length, namely the initial level of 0.45 mm and half of this value - 0.225 mm. The results are presented in Fig. 23. In the beginning, one should notice that the ultimate strength for a standard deviation of 0 is the basic model, where the uniform thickness reduction is assumed. In all cases, when considering thickness deviations within the specimen, the ultimate capacity occurred to be lower. Thus, the model where only a uniform thickness reduction is considered is revealed to be non-conservative. In the case of a higher correlation length (above 100 mm), the relationship between the thickness standard deviation and ultimate strength is relatively linear. However, in the case of lower correlations (7.1 mm and 32 mm), the dependency is more non-linear, and the reduction of the ultimate strength tends to be more rapid with the increase of the standard deviation.

The sensitivity analysis will be used in further analysis to obtain the optimum values of random field characteristics. Based on the convergence studies, the nine realisations of the random field for specified values of the standard deviation and correlation length were revealed to be enough to provide a stable mean value. The correlation length of 0.1 m was revealed to have the most severe impact on the ultimate strength reduction, and thus it will be considered in further studies.

6. Impact of initial plate thickness

The structural behaviour of corroded stiffened plates considering different thicknesses of the plate and the stiffener is studied in this section. Three different thicknesses are taken into account together with their statistical descriptors, as presented in Table 2. Two different levels of corrosion degree of degradation are considered, namely 10.5% and 21%. Figs. 24–26 show the force–displacement curves considering 5 mm, 6 mm and 8 mm thickness stiffened plates, respectively. The upper bunch of curves in each Figure represent the 10.5% level of corrosion degradation, whereas the lower bunch represent the high value of corrosion diminution.

Notably, the behaviour is almost identical to the bifurcation point in all cases where buckling occurs. From that point, some scatter in terms of force value starts to be visible. After reaching the bifurcation point, the curves are scattered, considering particular degree values of degradation. However, the highest scatter is observed in the region where a stiffened plate reaches its maximum capacity, leading to significant

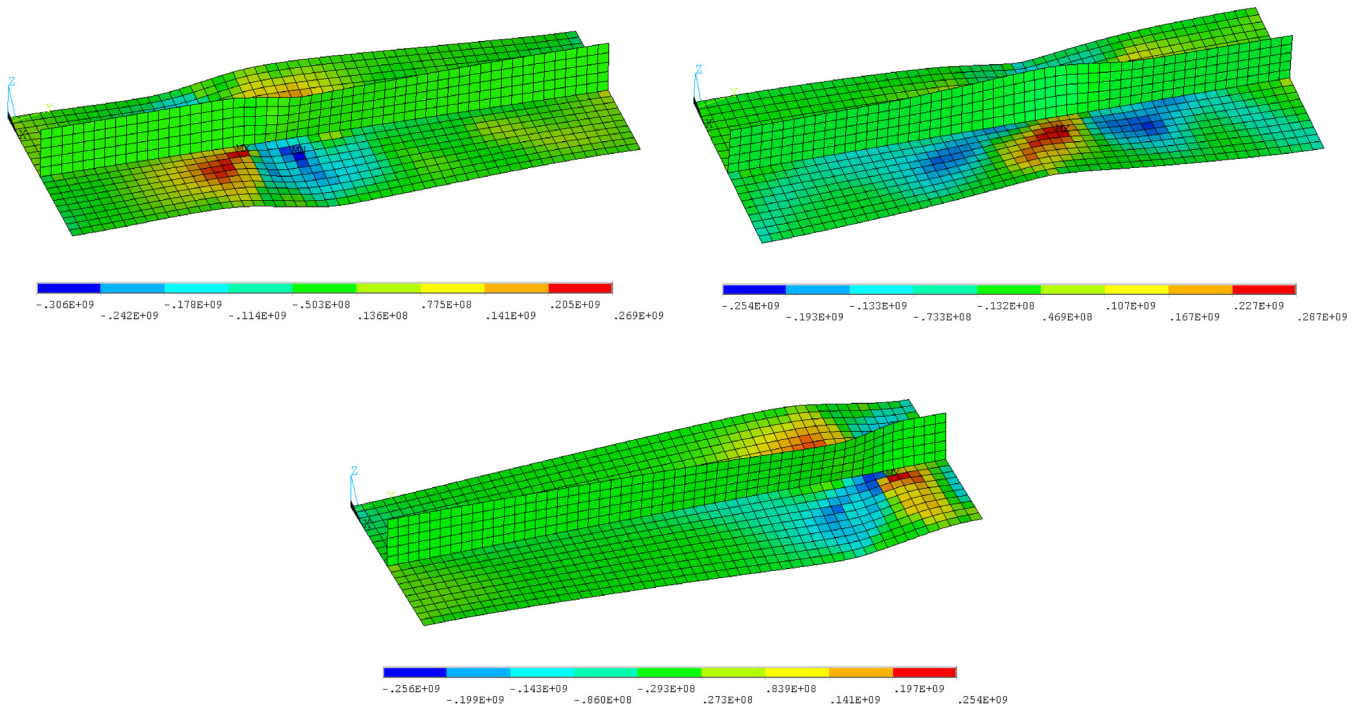

Fig. 22. Post-collapse shapes of specimens with low correlation (left up), moderate correlation (right up) and higher correlation (bottom), normal stresses [Pa].

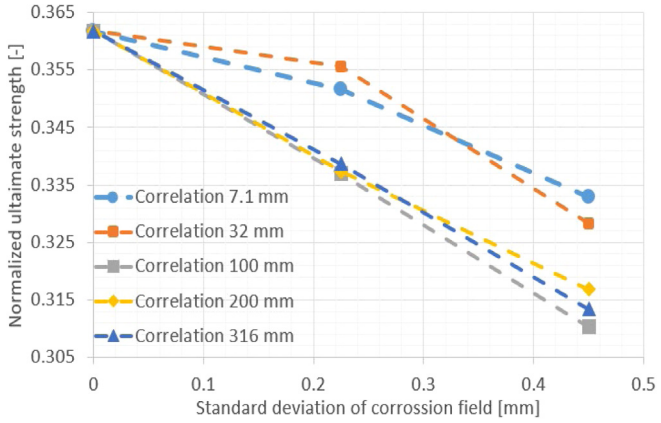

Fig. 23. Impact of random field standard deviation on the reduction of ultimate strength.

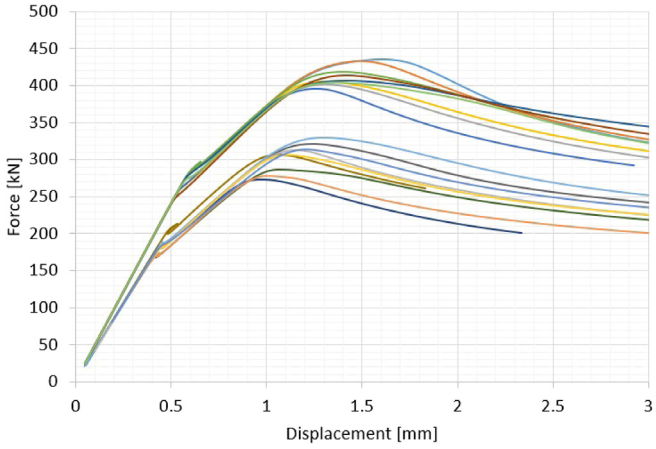

Fig. 25. Force–displacement relationships, 6 mm.

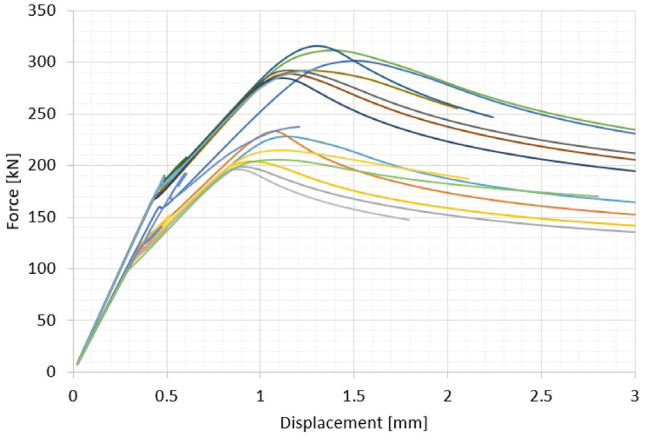

Fig. 24. Force–displacement relationships, 5 mm.

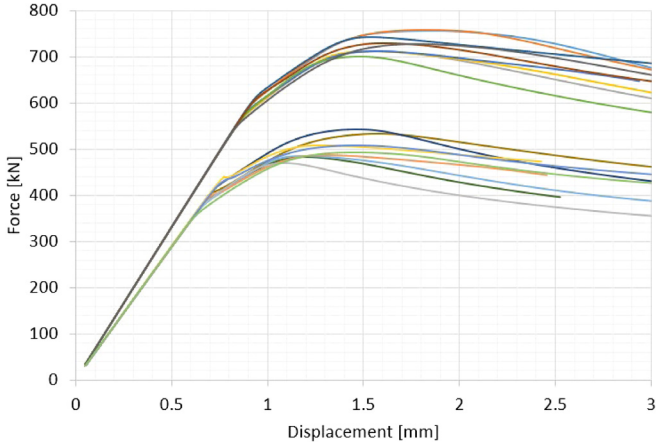

Fig. 26. Force–displacement relationships, 8 mm.

Table 3
Ultimate strength of corroded stiffened plates.

Thickness [mm]	DoD [%]	Mean ultimate force [kN]	Normalised ultimate strength [-]		
			Mean value	St. Dev.	COV [-]
5	10.5	297.1	0.414	0.014	0.035
	21	214.0	0.298	0.022	0.072
6	10.5	412.7	0.484	0.016	0.034
	21	303.1	0.355	0.023	0.064
8	10.5	727.4	0.504	0.014	0.028
	21	501.0	0.347	0.017	0.049

differences in ultimate strength values and post-collapse behaviour. Depending on the particular thickness distribution on the plate, which is correlated with the distribution of mechanical properties, the plate will collapse in different positions of the cross-section concerning its longitudinal direction, which was already observed in Fig. 22. One also needs to notice that with the increase of plate thickness, the scatter of ultimate strength becomes smaller. Apart from the thickness standard deviation being higher for thicker plates, the uncertainty level, compared to initial thickness, is lower for thicker plates. The statistical descriptors of the normalised ultimate strength are summarised in Table 3.

Based on the presented results, one can conclude that with the increasing level of corrosion degradation, the resulting uncertainty of ultimate strength increases. This is related to the increasing thickness variation with corrosion development. The Coefficient of Variation is between 2.8% and 7.2%, which can be classified as relatively high. The highest uncertainties are observed for the ultimate strength of 5 mm thick stiffened plates, whereas the capacity of 8 mm plates is subjected to the lowest uncertainty level. With the increase of plate thickness, the ultimate normalised strength also increases, which is related to the plate slenderness ratio. Compared to the intact specimens, the ultimate strength reduction for severely corroded stiffened plates reaches 50%.

7. Comparison with exact numerical results

In the presented section, the results of ultimate strength predictions that incorporated the random fields of corrosion are compared with numerical investigations that considered actual corrosion fields as analysed in Section 4. Namely, the maximum, mean and minimum results from random field analysis are compared with the exact FE analysis.

Fig. 27 presents the computations for 5 mm stiffened plates. It is noted that the results obtained via generated random fields are lower concerning the exact FE results, and there is also observed quite a high scatter of random results. The closest results regarding accurate FE analysis were obtained for maximum values of ultimate strength from random field analysis. However, the random field analysis was performed for correlation length that produced the lowest ultimate strength values. Probably, in an experiment, other correlations were observed.

The comparison for 6 mm plates is presented in Fig. 28. In this case, the results obtained from accurate FE analysis are close to the mean values of ultimate strength resulting from computations with randomly generated corrosion fields. This indicates that the random fields show the possible case of a real corrosion distribution. Fig. 29 shows the comparison made for 8 mm stiffened plates. It is noted that similarly to 5 mm plates, the exact results are closest to the maximum values from random field analysis. However, the numerical results for generated corrosion fields are not subjected to very high scatter in this case.

Based on the presented analysis, it is observed that the exact FE results and results based on the random field analysis are close to each other. Nevertheless, some differences are observed. The main reason should be the difference in thickness distributions since the mechanical properties were the same within the considered models. Thus, the corrosion fields generated randomly resulted in lower values of ultimate strength in general. This indicates that more significant areas of high thickness reductions existed when the corrosion field was

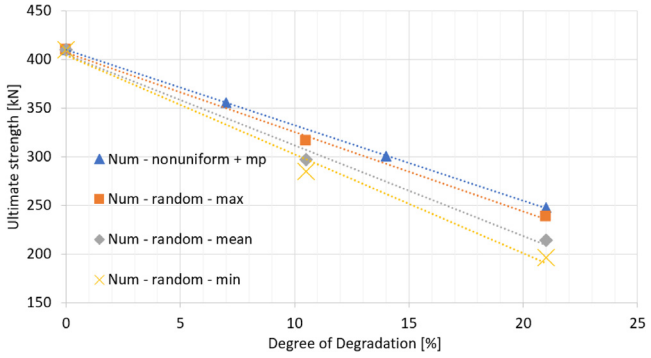

Fig. 27. Random field analysis and exact FE computations, 5 mm stiffened plates.

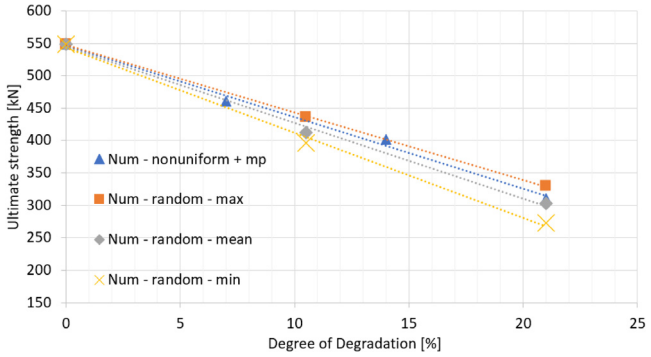

Fig. 28. Random field analysis and exact FE computations – 6 mm stiffened plates.

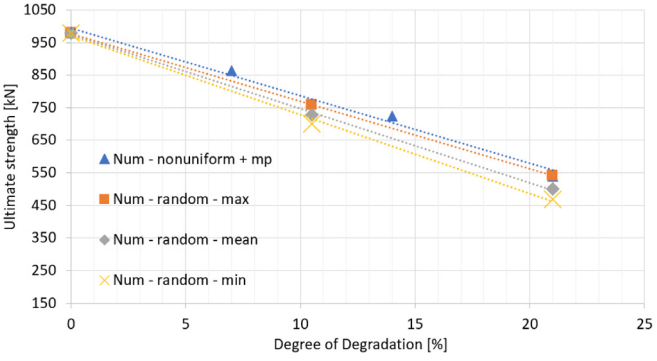

Fig. 29. Random field analysis and exact FE computations – 8 mm stiffened plates.

generated compared to measured ones in corroded specimens. Although for 5 mm and 8 mm plates, the measured corrosion fields seem to be not so critical for the reduction of ultimate strength compared to randomly generated fields, there seems to be reasonable from the safety point of view to take into account the representative random fields that result in the mean value of ultimate strength reduction. Especially in 6 mm plates, the exact FE analysis results were close to the mean ultimate

strength values from random field analysis. Thus, such corrosion fields could exist in real conditions.

8. Conclusions

The presented study investigated the impact of general corrosion degradation on the ultimate strength of stiffened plates. A newly developed model was proposed, which includes the spatial variation of thickness reduction in a macro-scale and subsequent reduction of mechanical properties to reflect the corrosion degradation impact on a micro-scale.

The model considering a uniform thickness reduction in corrosion degradation was revealed to be a non-conservative one in comparison to the model, taking into account the non-uniformity of the thickness of the corroded plate. When only thickness change is considered with corrosion development, the ultimate strength values can be overestimated by up to 30%. It needs to be noted that this type of model is commonly used in design practice. It has been shown that only when the non-uniform distribution of the thickness and changes in mechanical properties are considered in the numerical model are the results similar to those obtained via experiment. Nevertheless, some differences concerning the experiment were still visible due to the various sources of uncertainties (boundary conditions, mechanical properties, thickness measurements). Thus, implementing other effects, such as the eccentricity of the applied load, could be beneficial in the future. Additionally, the thickness distribution could be captured in more detail, and surface scanning (e.g., photogrammetry) could be employed.

Random field modelling was an excellent tool for simulating the actual fields of corrosion. This technique generates many cases without time-consuming, long-lasting, and difficult corrosion tests. Further, by generating many cases, some more sophisticated studies showing uncertainty levels could also be conducted. However, further validation studies are needed since there was observed bias between the exact numerical model and the random field approach. This should lead to a better representation of actual thickness distribution. The obtained uncertainties related to the ultimate capacity of corroded stiffened plates have the potential to be incorporated in the reliability analysis of such structures.

CRediT authorship contribution statement

Krzysztof Woloszyk: Validation, Methodology, Investigation, Formal analysis, Data curation, Conceptualization, Visualization, Writing – original draft, Writing – review & editing. **Yordan Garbatov:** Methodology, Conceptualization, Writing – original draft, Writing – review & editing.

Declaration of competing interest

The authors declare that they have no known competing financial interests or personal relationships that could have appeared to influence the work reported in this paper.

Data availability

Data will be made available on request.

Acknowledgements

This work has been supported by the National Science Centre, Poland (grant No. 2018/31/N/ST8/02380). The ANSYS software used in the presented simulations in this study was available as a part of the partnership cooperation agreement between ANSYS Inc., MESco sp. z o.o., and the Gdansk University of Technology.

References

[1] R. Melchers, Corrosion uncertainty modelling for steel structures, J. Constr. Steel Res. 52 (1999) 3–19.
[2] P. Pedeferri, Corrosion Science and Engineering, Springer International Publishing, Cham, 2018.
[3] J. Paik, J. Lee, M. Ko, Ultimate compressive strength of plate elements with pit corrosion wastage, Proc. Inst. Mech. Eng. M J. Eng. Marit. Environ. 217 (2003) 185–200.
[4] X. Jiang, C. Guedes Soares, Ultimate capacity of rectangular plates with partial depth pits under uniaxial loads, Mar. Struct. 26 (2012) 27–41.
[5] T. Nakai, H. Matsushita, N. Yamamoto, H. Arai, Effect of pitting corrosion on local strength of hold frames of bulk carriers (1st report), Mar. Struct. 17 (2004) 403–432.
[6] A. Rahbar-Ranji, N. Niamir, A. Zarookian, Ultimate strength of stiffened plates with pitting corrosion, Int. J. Nav. Archit. Ocean Eng. 7 (2015) 509–525.
[7] Y. Zhang, Y. Huang, Y. Wei, Ultimate strength experiment of hull structural plate with pitting corrosion damage under uniaxial compression, Ocean Eng. 130 (2017) 103–114.
[8] J. Zhang, X. Shi, C. Guedes Soares, Experimental analysis of residual ultimate strength of stiffened panels with pitting corrosion under compression, Eng. Struct. 152 (2017) 70–86.
[9] P. Domzalicki, I. Skalski, C. Guedes Soares, Y. Garbatov, Large scale corrosion tests, in: P. Das (Ed.), Anal. Des. Mar. Struct, Taylor & Francis Group, 2009, pp. 193–198.
[10] S. Saad-Eldeen, Y. Garbatov, C. Guedes Soares, Experimental assessment of the ultimate strength of a box girder subjected to severe corrosion, Mar. Struct. 24 (2011) 338–357.
[11] S. Saad-Eldeen, Y. Garbatov, C. Guedes Soares, Ultimate strength assessment of corroded box girders, Ocean Eng. 58 (2013) 35–47.
[12] S. Saad-Eldeen, Y. Garbatov, C. Soares, Ultimate strength of a corroded box girder subjected to pure bending and a non-propagating crack, in: Towar. Green Mar. Technol. Transp, CRC Press, 2015, pp. 373–380.
[13] Y. Garbatov, M. Tekgoz, C. Guedes Soares, Experimental and numerical strength assessment of stiffened plates subjected to severe non-uniform corrosion degradation and compressive load, Ships Offshore Struct. 12 (2017) 461–473.
[14] Y. Wang, S. Xu, A. Li, Flexural performance evaluation of corroded steel beams based on 3D corrosion morphology, Struct. Infrastruct. Eng. (2020) 1–16.
[15] Y. Garbatov, C. Guedes Soares, J. Parunov, J. Kodvanj, Tensile strength assessment of corroded small scale specimens, Corros. Sci. 85 (2014) 296–303.
[16] Y. Garbatov, J. Parunov, J. Kodvanj, S. Saad-Eldeen, C. Guedes Soares, Experimental assessment of tensile strength of corroded steel specimens subjected to sandblast and sandpaper cleaning, Mar. Struct. 49 (2016) 18–30.
[17] Y. Wang, S. Xu, H. Wang, A. Li, Predicting the residual strength and deformability of corroded steel plate based on the corrosion morphology, Constr. Build Mater. 152 (2017) 777–793.
[18] B. Nie, S. Xu, J. Yu, H. Zhang, Experimental investigation of mechanical properties of corroded cold-formed steels, J. Constr. Steel Res. 162 (2019) 105706.
[19] G. Qin, S. Xu, D. Yao, Z. Zhang, Study on the degradation of mechanical properties of corroded steel plates based on surface topography, J. Constr. Steel Res. 125 (2016) 205–217.
[20] K. Woloszyk, M. Kahsin, Y. Garbatov, Numerical assessment of ultimate strength of severe corroded stiffened plates, Eng. Struct. 168 (2018) 346–354.
[21] Y. Garbatov, C. Guedes Soares, G. Wang, Nonlinear time-dependent corrosion wastage of deck plates of ballast and cargo tanks of tankers, J. Offshore Mech. Arct. Eng. 129 (2006) 48–55.
[22] K. Woloszyk, Y. Garbatov, J. Kowalski, Indoor accelerated controlled corrosion degradation test of small- and large-scale specimens, Ocean Eng. 241 (2021) 110039.
[23] R. Jankowski, H. Walukiewicz, Modeling of two-dimensional random fields, Probabilistic Eng. Mech. 12 (1997) 115–121.
[24] J. Górski, T. Mikulski, M. Oziębło, K. Winkelmann, Effect of geometric imperfections on aluminium silo capacities, Stahlbau 84 (2015) 52–57.
[25] J. Górski, K. Winkelmann, Generation of random fields to reflect material and geometric imperfections of plates and shells, in: Shell Struct. Theory Appl., Vol. 4, CRC Press, 2017, pp. 537–540.
[26] A. Teixeira, C. Guedes Soares, Ultimate strength of plates with random fields of corrosion, Struct. Infrastruct. Eng. 4 (2008) 363–370.
[27] D. Georgiadis, M. Samuelides, The effect of corrosion spatial randomness and model selection on the ultimate strength of stiffened panels, Ships Offshore Struct. 16 (2021) 140–152.
[28] K. Woloszyk, Y. Garbatov, Random field modelling of mechanical behaviour of corroded thin steel plate specimens, Eng. Struct. 212 (2020) 110544.
[29] K. Woloszyk, Y. Garbatov, An enhanced method in predicting tensile behaviour of corroded thick steel plate specimens by using random field approach, Ocean Eng. 213 (2020) 107803.

[30] K. Woloszyk, Y. Garbatov, J. Kowalski, Experimental ultimate strength assessment of stiffened plates subjected to marine immersed corrosion, Appl. Ocean Res. (2022) Submitted.
[31] K. Woloszyk, Y. Garbatov, P. Kłosowski, Stress–strain model of lower corroded steel plates of normal strength for fitness-for-purpose analyses, Constr. Build Mater. 323 (2022) 126560.
[32] ANSYS, Online manuals, release 19, 2019.
[33] International Association of Classification Societies. P.R. No 19, Procedural Requirement for Thickness Measurements, 2017.
[34] K. Woloszyk, P. Bielski, Y. Garbatov, T. Mikulski, Photogrammetry image-based approach for imperfect structure modelling and FE analysis, Ocean Eng. 223 (2021) 108665.
[35] K. Woloszyk, Y. Garbatov, J. Kowalski, L. Samson, Numerical and experimental study on effect of boundary conditions during testing of stiffened plates subjected to compressive loads, Eng. Struct. 235 (2021) 112027.
[36] R. Ghanem, P. Spanos, Stochastic Finite Elements: A Spectral Approach, Springer New York, New York, NY, 1991.
[37] C. Li, A. Der Kiureghian, Optimal discretization of random fields, J. Eng. Mech. 119 (1993) 1136–1154.
[38] Mathworks, Matlab R2019b, 2019.
[39] Constantine P. Random field simulation, 2012, https://Www.Mathworks.Com/Matlabcentral/Fileexchange/27613-Random-Field-Simulation. (Accessed 26 November 2019).
[40] S. Smith, Influence of local compressive failure on ultimate longitudinal strength of a ship's hull, Proc. Int. Sym. Pract. Des. Shipbuild. (1977) 73–79.
[41] Y. Garbatov, C. Guedes Soares, K. Masubuchi, Residual stresses and distortion in welds, in: Ref. Modul. Mater. Sci. Mater. Eng., Elsevier, 2016.
[42] C. Guedes Soares, Y. Garbatov, A. Zayed, G. Wang, Corrosion wastage model for ship crude oil tanks, Corros. Sci. 50 (2008) 3095–3106.